Hyperspectral characterization of tissue simulating phantoms using a supercontinuum laser in a spatial frequency domain imaging instrument

Mohammad Torabzadeh[a,b], Patrick Stockton[c], Gordon T. Kennedy[a], Rolf B. Saager[a], Anthony J. Durkin[a,b], Randy A. Bartels[c], Bruce J. Tromberg[a,b]*
[a]Laser Microbeam and Medical Program, Beckman Laser Institute, Irvine, CA, USA 92612
[b]University of California Irvine, Department of Biomedical Engineering, Irvine, CA, USA 92697
[c]Colorado State University, School of Biomedical Engineering, Fort Collins, CO, USA 80523

ABSTRACT

Hyperspectral Imaging (HSI) is a growing field in tissue optics due to its ability to collect continuous spectral features of a sample without a contact probe. Spatial Frequency Domain Imaging (SFDI) is a non-contact wide-field spectral imaging technique that is used to quantitatively characterize tissue structure and chromophore concentration. In this study, we designed a Hyperspectral SFDI (H-SFDI) instrument which integrated a supercontinuum laser source to a wavelength tuning optical configuration and a sCMOS camera to extract spatial (Field of View: 2cm×2cm) and broadband spectral features (580nm-950nm). A preliminary experiment was also performed to integrate the hyperspectral projection unit to a compressed single pixel camera and Light Labeling (LiLa) technique.

Keywords: tissue optical properties, spatial frequency domain imaging, scattering, hyperspectral imaging, supercontinuum laser

* Bruce J. Tromberg, bjtrombe@uci.edu

1 INTRODUCTION

Human skin and subcutaneous tissue is a composition of multiple chromophores mainly melanin, oxy/deoxy/methemoglobin, fat and water. Since these species have overlapping absorption features in the visible and near infrared regions, accurate quantification of their concentrations requires multiple spectral data points. In this regard, Hyperspectral Imaging (HSI) is a superior tool that provides continuous spectral output and can enhance chromophore fitting based on absorption coefficients at multiple wavelengths. To achieve accurate absorption coefficient values at each wavelength, contribution of tissue scattering needs to be subtracted from raw reflectance data.

Spatial frequency domain imaging (SFDI) is a tissue spectroscopic imaging technique that decouples absorption from scattering by projecting structured illumination (1-4) at multiple spatial frequencies onto a sample and captures diffuse reflectance light with a camera (5, 6). SFDI has potentials to be implemented in a variety of areas including wound healing, skin lesions, and immune response (7-14).We have developed a hyperspectral light projection unit of a SFDI system which is powered by a supercontinuum laser and a wavelength-tuning optical configuration. The proposed hyperspectral SFDI system extracts tissue optical properties, absorption and reduced scattering, at extremely fine spectral resolution in the 580-950nm region.

Here, we perform tissue simulating phantom studies to demonstrate sensitivity of optical property extraction in a broad spectral region. We also investigated potentials of the hyperspectral projection unit to be integrated to a compressed single pixel camera and Light Labeling (LiLa) technique.

Design and Quality for Biomedical Technologies XI, edited by Ramesh Raghavachari, Rongguang Liang, Proc. of SPIE Vol. 10486, 104860G · © 2018 SPIE · CCC code: 1605-7422/18/$18 · doi: 10.1117/12.2291369

2 HYPERSPECTRAL SFDI INSTRUMENT

The core of our hyperspectral SFDI instrument is a supercontinuum laser source (SC 400-2, Fianium, Southampton, UK) which gives continuous spectral output in the 400-2100nm range with total power of 2 Watts. A folded Martinez compressor is designed to bandpass filter the output of laser source. In this configuration, a prism disperses the beam on a Plössl lens which brings the light to a line focus. A fixed slit on a linear stage is then used to sweep through the line focus, thus selecting different spectral bins. The wavelength-tuned beam is expanded via a telescope and imaged onto a Digital Micro-Mirror Device (DMD) which spatially modulates the light and projects sinusoidal pattern at fixed spatial frequency and at multiple phases (0°,120° ,240°) onto a tissue phantom sample. Diffuse reflected light from the sample is finally detected using a high speed scientific complementary metal oxide semiconductor (sCMOS) camera (ORCA-Flash 4.0 V2, Hamamatsu Photonics K.K., Japan). Figure 1 shows a schematic of the H-SFDI instrument.

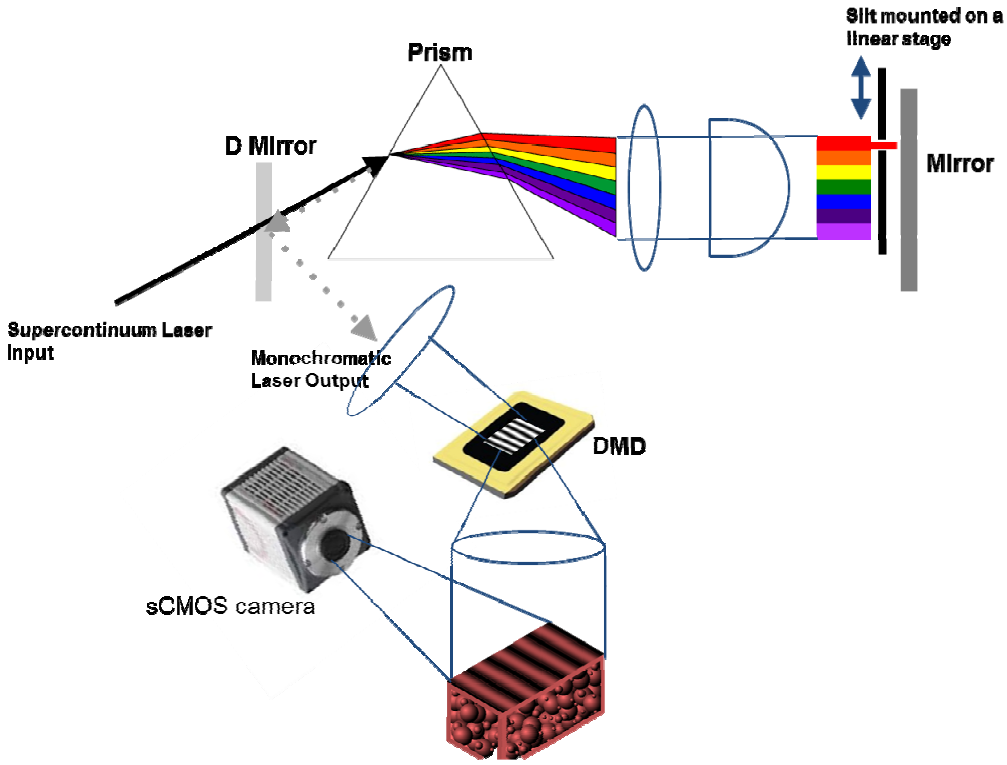

Fig. 1 Schematic of the H-SFDI instrument.

3 PHANTOM MEASUREMENT

We performed a series of tissue phantom measurements to assess performance of the H-SFDI instrument to extract optical properties in a broad spectral range. We built a silicone-based phantom with titanium dioxide (TiO_2) as scattering agent and India ink as absorptive agent (15, 16). We then inserted a cylindrical mold in the base phantom. Once the base phantom is cured, we removed the mold and poured 5 different solutions in the resulting hole, one at a time, and measured using the H-SFDI instrument. We have used acetone soluble FHI5832 (Fabricolor Holding Int'l, Paterson, New Jersey), water-soluble blue food coloring (Ateco, Glen Cove, New York), water-soluble naphthol green b (Sigma Aldrich, St. Louis, Missouri), and water soluble FHI96715 (Fabricolor Holding Int'l, Paterson, New Jersey). These dyes have absorption peaks at 564, 638, 730, and 900nm respectively. To make a turbid version of these solutions and decouple their scattering and absorption properties using the H-SFDI instrument, we added 1mL of 20% Intralipid (Fresenius Kabi, Uppsala, Sweden) to 19mL of each solution to achieve 1% Intralipid

concentration in each of them. We added water-diluted acetone to our FHI5832 dye. The 5th sample that we measured was extra-virgin olive oil with absorption peaks at 675 and 920nm. We added known amount of sonicated TiO_2 powder to olive oil to introduce turbidity and therefore light scattering properties. These 5 samples were measured using the H-SFDI instrument in the 580-950nm range at 1000 spectral bins. As it is shown in Fig 2(a), the absorption spectra shape of these samples match with their expected absorption spectra. Absorption contribution from the main solvent, water, is also detected for the first 4 solution at wavelengths longer than 850nm. These 5 samples have been calibrated against a silicone-based phantom with known optical properties which naturally shows an absorption increase in the 890-910nm range. Since we noticed a dip in absorption values for these samples in the same spectral region, we believe there may be some cross-talk between each sample and its calibration phantom. Figure 2(b) shows reduced scattering spectra for these 5 samples. As it was expected, dominant scattering properties of the water-soluble dyes arise from Intralipid. Since these solutions possess similar Intralipid concentrations, their reduced scattering spectra line up with each other.

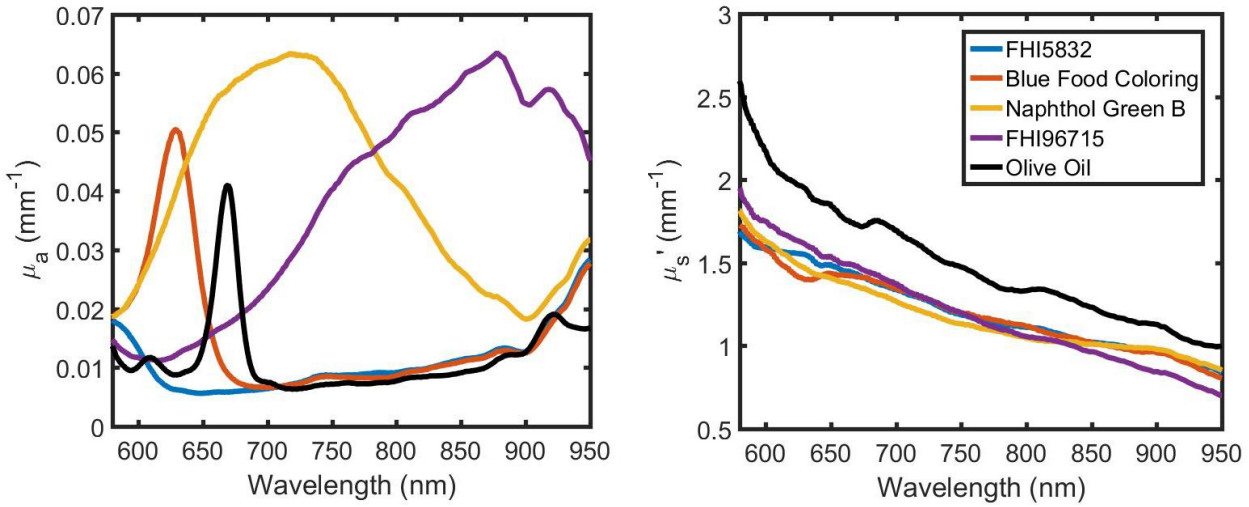

Fig. 2 (a) Plot of bulk μ_a spectra and (b) μ_s' spectra for 5 samples: 3 water-soluble dyes 1 acetone-soluble dye with 1% Intralipid concentration, and olive oil.

Figure 3 shows absorption coefficient maps at five different spectral bins. The initial optical design of the H-SFDI instrument was to produce a 4cm×6cm Field of View (FOV). However, we noticed spatial heterogeneity in calibrated reflectance maps which eventually could cause artifacts in both absorption and reduced scattering maps. We therefore narrowed down the FOV to a central 2cm×2cm crop of the initial FOV.

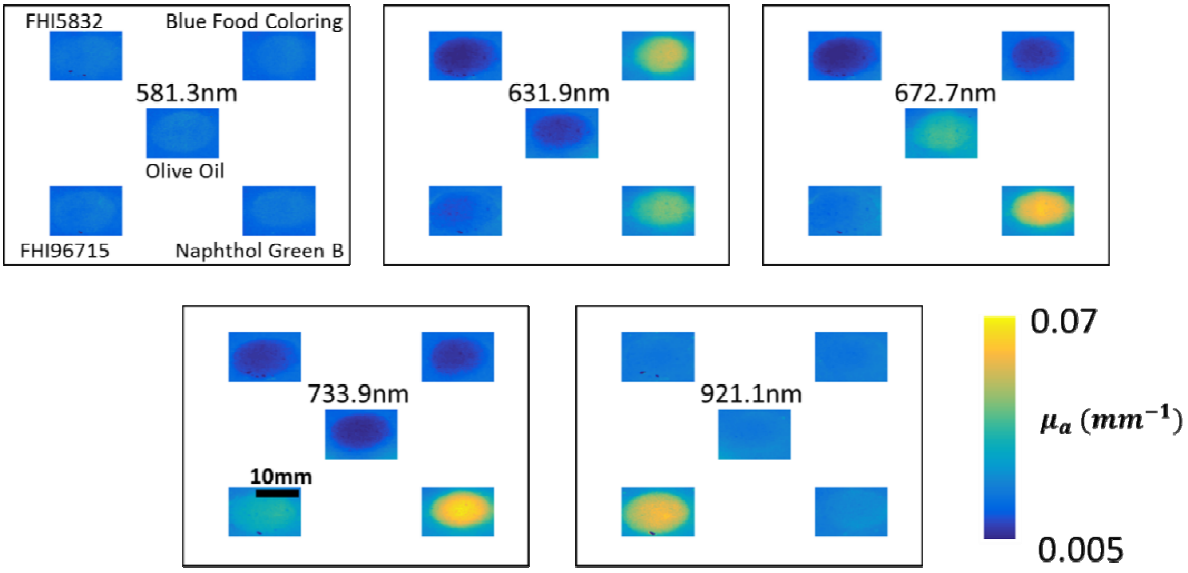

Fig. 3 μ_a maps of sample at 6 wavelengths.

4 INTEGRATIONS TO SINGLE PIXEL CAMERA AND LIGHT LABELING

While we mainly focused on a time-domain scanning technique and focal array sensor in the previous section, the hyperspectral projection unit can also be implemented to a frequency-domain technique where each spectral bin is temporally modulated at a distinct frequency. Hyperspectral information is encoded in the illumination beam by temporal modulation, so-called Light Labeling (LiLa) (17). LiLa works by uniquely modulating each spectral component with a temporal frequency. The light labeling can be thought of from a communication theory perspective, where each modulation frequency represents a channel and each channel contains spectral information. The channels can be multiplexed because they form an orthogonal basis. It is well known that sinusoids produce an orthogonal basis, which means each spectral component can be readily recovered by projecting the time signal onto a sinusoidal basis, that is, taking the Fourier transform of the time signal will recover the power spectrum. It was shown in that LiLa can be used with a conventional 2D array detector (18), however, this method is very slow and requires hundreds of images to be acquired to recover the spectral information (19). If, instead, a single element detector is used for detection, the large bandwidth may be leveraged to rapidly acquire the spectral information while simultaneously obtaining the 2D information using a single pixel camera. An additional advantage of the single element detector is that a broad range of detectors that may be used to capture spectral information outside of the visible band where traditional 2D detectors fall short in terms of SNR, pixel density, cost, and availability. We previously assessed the single pixel camera performance in the context of a multi-spectral SFDI instrument (20). We showed agreement in optical property extraction using a conventional camera and the single pixel approach. Compressed Sensing (CS) technique was used to decrease total number of measurements required to reconstruct an image using the single pixel camera. In a single pixel hyperspectral SFDI instrument, LiLa is achieved through mounting a spinning disk reticle at the focal plane of the folded Martinez compressor.

We performed preliminary tissue phantom measurement to reconstruct images using a single pixel camera with CS technique (21), and spectrally encoded supercontinuum output using LiLa. Figure 4 shows image reconstructions at 8 spectral bins with approximate bandwidth of 30nm. One side of the silicone based tissue phantom is made of naphthol green b as absorptive agent and TiO_2 as scattering agent. The other side of the phantom is Spectralon (Spectralon, Lab Sphere, North Sutton, New Hampshire) with theoretical 99% reflectance. The reconstructed images were 64×64 in pixel resolution with compression ratio of 5. DC pattern is projected onto the sample in this measurement.

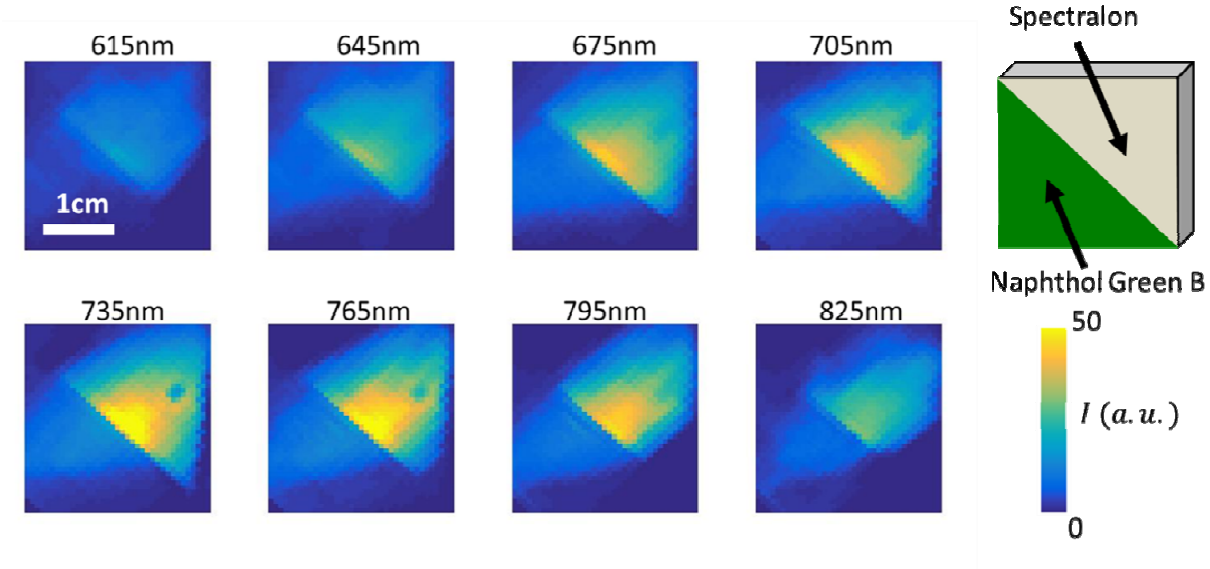

Fig. 4 Reflectance maps at 8 spectral bins (Bandwidth=30nm) and schematic of phantom

At each spectral bin, we chose an ROI on two sides of the phantom and calibrated the naphthol green b portion by dividing it's measured reflectance intensity by the reflectance intensity that was measured for the Spectralon. We then corrected for the contribution of scattering properties using a Monte Carlo (MC) simulation of radiative transfer turbid medium and calculated absorption coefficients at multiple spectral bins. As will be discussed in this section, we observed poor reconstruction quality at AC frames of SFDI workflow and therefore estimated scattering values from the known TiO_2 concentration. Figure 5 is a plot of the absorption spectrum for the naphthol green b phantom. The extracted values follow trend of the spectrum of naphthol green b in silicone.

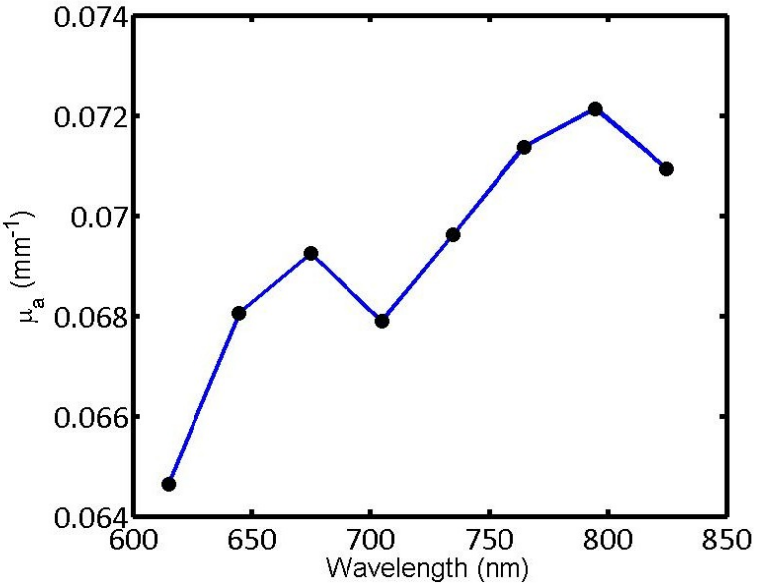

Fig. 5 μ_a at 8 spectral bins acquired using the single pixel hyperspectral SFDI instrument

One of challenges associated with integrating the light-labeling H-SFDI instrument into our compressed single pixel camera was susceptibility of image reconstructions to subtle temporal/spectral oscillations in the supercontinuum source output. What considers to be sampling contrast from one random pattern on the single pixel camera to

another random pattern can be about 8% difference in photodiode intensity output depending on measurement phantom. A stack of these intensity values acquired from the photodiode of the camera are finally inserted to a CS algorithm for image reconstruction. However, we confronted 1-2% random source noise both spectrally and temporally, which distorted the CS reconstructed images when it came to SFDI workflow. In particular, this was a problem with respect to the reconstruction of AC frames. In future work, other intensity calibration approaches in the frequency domain can be applied to this instrument so that raw reflectance images provide enough signal-to-noise Ratio (SNR) for accurate quantification of optical properties.

5 CONCLUSION

We developed a hyperspectral SFDI (H-SFDI) instrument by integrating a supercontinuum laser source to a wavelength-tuning optical configuration and pattern projection unit. Using a high-speed sCMOS camera, this system allowed us to calculate tissue phantom's optical properties, absorption and reduced scattering, over a 2cm×2cm FOV at more than 1000 spectral bins. Future work will emphasize validation of the optical property values achieved using the H-SFDI instrument against results from a conventional spectrophotometer. Imaging speed is another area that needs to be improved. The slit mounted on a linear stage is a limiting factor in terms of achieving sub-second image-cube acquisition. Other line scanning techniques such as using a spiral function print on a rotating disk can potentially improve imaging speed.

We also explored utilizing the LiLa technique to simultaneously encode multiple spectral bins in the frequency domain. A single pixel camera powered by CS technique was then used on the detection side to decode each spectral component and reconstruct images of them. Although the single pixel H-SFDI suffered from low SNR due to laser source oscillations and wobbling noise from the LiLa disk, we managed to reconstruct images of a heterogeneous tissue phantom at multiple spectral bins. These results suggest that our versatile H-SFDI instrument powered by a supercontinuum laser source provides a framework to quantify tissues optical properties in a broad spectral range and at extremely fine spectral resolution. This can open an opportunity to rigorously look for additional tissue chromophores such as fat, water, and collagen which play an important role in applications such as wound healing and inflammation.

ACKNOWLEDGMENTS

The authors gratefully acknowledge funding provided by the NIH NIBIB Biomedical Technology Research Center LAMMP: P41EB015890, the NIH Grant R21EB020953, the Military Medical Photonics Program: AFOSR Grant No. FA9550-17-1-0193, and Arnold and Mabel Beckman Foundation.

REFERENCES

[1] Cuccia, D.J., Bevilacqua, F., Durkin, A.J., and Tromberg, B.J., "Modulated imaging: quantitative analysis and tomography of turbid media in the spatial-frequency domain," Optics letters 30(11), 1354 (2005).

[2] Bélanger, S., Abran, M., Intes, X., Casanova, C., and Lesage, F., "Real-time diffuse optical tomography based on structured illumination," Journal of biomedical optics 15(1), 016006 (2010).

[3] Zeng, J., Albooyeh, M., Darvishzadeh-Varcheie, M., Kamandi, M., Veysi, M., Hanifeh, M., Rajaei, M., Albee, B., Potma, E.O., et al., "Unveiling magnetic and chiral nanoscale properties using structured light and nanoantennas," 11th International Congress on Engineered Materials Platforms for Novel Wave Phenomena, (2017).

[4] Guclu, C., Veysi, M., Darvishzadeh-Varcheie, M., and Capolino, F., "Artificial Magnetism via Nanoantennas under Azimuthally Polarized Vector Beam Illumination," Conference on Lasers and Electro-Optics, (2016).

[5] Cuccia, D.J., Bevilacqua, F., Durkin, A.J., Ayers, F.R., and Tromberg, B.J., "Quantitation and mapping of tissue optical properties using modulated imaging," Journal of biomedical optics 14(2), 024012 (2009).

[6] Wilson, R.H., Crouzet, C., Torabzadeh, M., Bazrafkan, A., Farahabadi, M.H., Jamasian, B., Donga, D., Alcocer, J., Zaher, S.M., et al., "High-speed spatial frequency domain imaging of rat cortex detects dynamic optical and physiological properties following cardiac arrest and resuscitation," Neurophotonics 4(4), 045008 (2017).

[7] Yafi, A., Muakkassa, F.K., Pasupneti, T., Fulton, J., Cuccia, D.J., Mazhar, A., Blasiole, K.N., and Mostow, E.N., "Quantitative skin assessment using spatial frequency domain imaging (SFDI) in patients with or at high risk for pressure ulcers," Lasers in surgery and medicine 49(9), 827–834 (2017).

[8] Rohrbach, D.J., Muffoletto, D., Huihui, J., Saager, R., Keymel, K., Paquette, A., Morgan, J., Zeitouni, N., and Sunar, U., "Preoperative mapping of nonmelanoma skin cancer using spatial frequency domain and ultrasound imaging," Academic radiology 21(2), 263–270 (2014).

[9] Najdahmadi, A., Lakey, J.R.T., Botvinick, E., "Diffusion coefficient of alginate microcapsules used in pancreatic islet transplantation, a method to cure type 1 diabetes," Proc. SPIE 10506, 1050649 (2018).

[10] Nguyen, J.Q., Crouzet, C., Mai, T., Riola, K., Uchitel, D., Liaw, L.-H., Bernal, N., Ponticorvo, A., Choi, B., et al., "Spatial frequency domain imaging of burn wounds in a preclinical model of graded burn severity," Journal of biomedical optics 18(6), 066010 (2013).

[11] Najdahmadi, A., Gurlin, R.E., Weidling, J., White, S., Shergill, B., Lakey, J.R.T., Botvinick, E., "Non invasive study of oxygen tension and vascularization in subcutaneously implanted medical devices," Proc. SPIE 10488, 1048847 (2018).

[12] Nguyen, T.T.A., Ramella-Roman, J.C., Moffatt, L.T., Ortiz, R.T., Jordan, M.H., and Shupp, J.W., "Novel application of a spatial frequency domain imaging system to determine signature spectral differences between infected and noninfected burn wounds," Journal of burn care & research: official publication of the American Burn Association 34(1), 44–50 (2013).

[13] Najdahmadi, A., Zarei-Hanzaki, A., and Farghadani, E., "Mechanical properties enhancement in Ti–29Nb–13Ta–4.6Zr alloy via heat treatment with no detrimental effect on its biocompatibility," Materials & design 54, 786–791 (2014).

[14] Ponticorvo, A., Burmeister, D.M., Rowland, R., Baldado, M., Kennedy, G.T., Saager, R., Bernal, N., Choi, B., and Durkin, A.J., "Quantitative long-term measurements of burns in a rat model using Spatial Frequency Domain Imaging (SFDI) and Laser Speckle Imaging (LSI)," Lasers in surgery and medicine 49(3), 293–304 (2017).

[15] Ayers, F., Grant, A., Kuo, D., Cuccia, D.J., and Durkin, A.J., "Fabrication and characterization of silicone-based tissue phantoms with tunable optical properties in the visible and near infrared domain," Proc. SPIE 6870, 687007 (2008).

[16] Saager, R.B., Kondru, C., Au, K., Sry, K., Ayers, F., and Durkin, A.J., "Multilayer silicone phantoms for the evaluation of quantitative optical techniques in skin imaging," Proc. SPIE 7567, 756706 (2010).

[17] Domingue, S.R., Winters, D.G., and Bartels, R.A., "Light labeling with temporal intensity modulations for hyperspectral imaging," Proc. SPIE 9711, 971115 (2016).

[18] Applegate, M.B., and Roblyer, D., "High-speed spatial frequency domain imaging with temporally modulated light," Journal of biomedical optics 22(7), 76019 (2017).

[19] Domingue, S.R., Winters, D.G., and Bartels, R.A., "Hyperspectral imaging via labeled excitation light and background-free absorption spectroscopy," Optica 2(11), 929 (2015).

[20] Torabzadeh, M., Park, I.-Y., Bartels, R.A., Durkin, A.J., and Tromberg, B.J., "Compressed single pixel imaging in the spatial frequency domain," Journal of biomedical optics 22(3), 30501 (2017).

[21] Duarte, M.F., Davenport, M.A., Takhar, D., Laska, J.N., Sun, T., Kelly, K.F., and Baraniuk, R.G., "Single-pixel imaging via compressive sampling," IEEE Signal Processing Magazine 25(2), 83–91 (2008).